

# A Mean Optimization Filter to Improve Bluetooth AoA Indoor Positioning Accuracy for Ship Environments

Qianfeng Lin<sup>1</sup>, Jooyoung Son<sup>2,\*</sup> and Hyeongseol Shin<sup>3</sup>

<sup>1</sup>Department of Computer Engineering, Korea Maritime and Ocean University, 727 Taejong-ro, Yeongdo-Gu, Busan 49112, South Korea

<sup>2</sup>Division of Marine IT Engineering, Korea Maritime and Ocean University, 727 Taejong-ro, Yeongdo-Gu, Busan 49112, South Korea

<sup>3</sup>Department of Institutional, Korea Maritime and Ocean University, 727 Taejong-ro, Yeongdo-Gu, Busan 49112, South Korea

## Abstract

Currently, the most effective way to reduce transmission of COVID-19 is to differentiate between close contacts. Location points of close contact are essential for differentiation. As a major mode of transportation, ships provide a vehicle for virus transmission. Timely detection location of close contacts inside a ship can prevent the spread of viruses. Location-based services can be provided for ship passengers. Bluetooth is widely available in many wearable devices. The Bluetooth 5.1 angle of arrival (AoA) indoor positioning algorithms can provide a certain indoor positioning accuracy for ship passengers. The two most essential parameters in Bluetooth 5.1 AoA indoor positioning are elevation angle and azimuth angle. Elevation and azimuth are often not accurate enough due to noise, which increases indoor positioning errors. As a result, this paper proposes a mean optimization filter for ship environments, which combines the box plot method to improve Bluetooth 5.1 AoA indoor positioning accuracy, with an RMSE of 0.34 m.

## Keywords

Angle of arrival, Bluetooth 5.1, indoor positioning, ship environments

## 1. Introduction

COVID-19 pandemic has been significantly impacting cruise operations worldwide. These essential economic and employment activities will be gradually resumed. Cruise operators must ensure that ship passengers do not have unacceptable health risks. Ship spatial environment facilitates the spread of the virus during a global COVID-19 pandemic. A cruise ship has contributed to the spread of COVID-19 worldwide [1]. A former passenger of the Diamond Princess tested positive for COVID-19 [2]. The Japanese government ordered ship passengers and crew to enter a two-week quarantine. Due to the cramped working environment, crew members are among the occupational groups most susceptible to outbreaks of this virus [3]. Indoor positioning algorithms are capable of providing location services to ship passengers. This allows close contacts to be distinguished. As a result of the ship's complex indoor environment,

---


*IPIN 2022 WiP Proceedings, September 5 - 7, 2022, Beijing, China*

\*Corresponding author.

✉ linqianfeng@g.kmou.ac.kr (Q. Lin); mmlab@kmou.ac.kr (J. Son); tlgudtjf123@naver.com (H. Shin)

🆔 0000-0003-3770-3204 (Q. Lin); 0000-0001-7851-9214 (J. Son)

© 2022 Copyright for this paper by its authors. Use permitted under Creative Commons License Attribution 4.0 International (CC BY 4.0).

 CEUR Workshop Proceedings (CEUR-WS.org)

indoor positioning accuracy can be improved. This paper proposes a mean optimization filter (MOF) to improve the accuracy of the Bluetooth 5.1 AoA indoor positioning algorithm. The proposed method in this paper is applicable to devices that support Bluetooth 5.1 AoA. Therefore, the method proposed in this paper can be applied to scenarios that require location-based services.

## 2. Previous Works

Bluetooth is present in a wide variety of wearable devices. It can be used to get the location point of ship passengers easily. The Bluetooth 5.1 AoA indoor positioning technology provides precise location points of user devices. Research on this topic has been extensive.

[4] analyzes high-precision location services of direction-finding capabilities. Using Bluetooth 5.1 AoA receivers for direction finding, [5] studies a performance evaluation framework. [6] introduces a method that uses deep neural networks to estimate the location point of a Bluetooth Low Energy (BLE) transmitter (tag) based on the characteristics of the received signals at multiple anchor points (APs). The estimated AoA is then fed into the indoor positioning engine, which uses the least squares (LS) algorithm to estimate the tag's location point. [7] provides an experimental demonstration of indoor localization using Bluetooth 5.1 and software-defined radios. [8] provides BLE localization with carrier frequency offset mitigation based on AoA. Based on simulations, [9] evaluates a novel Bluetooth 5.1 AoA approach for low-cost indoor vehicle tracking. According to [10], AoA estimation is based on BLE transmissions when the multipath effect is present. [11] proposes a new localization algorithm that iterates between AoA estimation and multilateration steps to refine the estimated location points. They also develop a localization scenario for the assessment and validation of the algorithm in BLE sensor networks. Electromagnetic wave signals are more complex in ship environments. Signal noise can adversely affect indoor positioning accuracy. The two most important positioning parameters in Bluetooth 5.1 AoA are elevation and azimuth. As a result of the multipath effect, the elevation and azimuth collected by the AoA Locator differ significantly from the actual values. Therefore, this paper presents a MOF applicable to ship environments to determine the optimal average by continuously narrowing the range of possible angles.

## 3. Bluetooth 5.1 AoA Theory

The Bluetooth direction finding is based on the principle of AoA. When two antennas receive one another, angular phase shifts are produced. Antenna arrays can be used on either side of the communication link to determine phase shift and calculate location points. The receiver of AoA systems calculates the direction of the signal by measuring the phase shift of the incoming signal. Figure 1 shows what AoA is, and Figure 2 illustrates the method of measuring AoA [12].

In Bluetooth, AoA is implemented using CTE (Constant Tone Extension). As an unmodulated carrier in an offset format or a sequence of modulated 1s in an unwhitened format. The CTE is appended to the packet. Bluetooth LE uses the Gaussian Frequency Shift Keying (GFSK) modulation changes continuously throughout the packet to distinguish the different symbols (0 or 1). Without a stable frequency, the receiver cannot estimate the phase of the signal. When

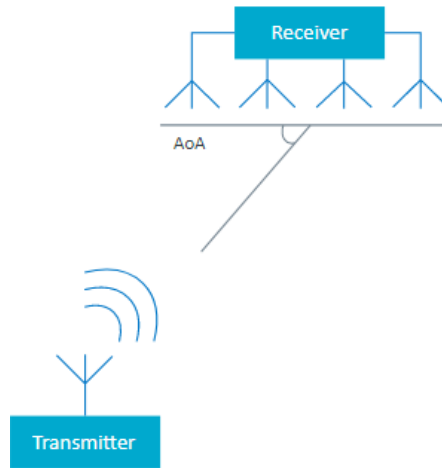


**Figure 1:** AoA method [12]

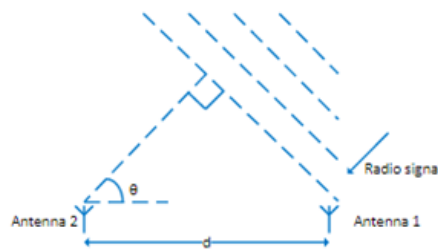


**Figure 2:** Measuring AoA [12]

calculating the AoA, it is necessary to take into account the 250 kHz difference between the CTE and the channel center frequency [12]. The Bluetooth direction finding uses IQ sampling, an in-phase and quadrature sampling technique, to determine the phase of incoming signals. In the receiver, the incoming signal is mixed with the local oscillator (LO) at 0 and 90 degrees off. It produces two orthogonal functions, an in-phase and quadrature components. I and Q components can be used to find the amplitude and phase of the Bluetooth signal. The receiver switches antennas to find the direction of the transmitter using the AoA method [12].

The transmitter inserts a constant frequency into a specific portion of CTE. Figure 3 illustrates the CTE structure. By sampling its IQ components, the receiver can determine the waveform phase. For multiple antennas, the receiver can calculate AoA. In order to reduce the influence of phase shift, IQ sampling of individual antennas in the reference period is required. To obtain the difference due to phase shift with a certain location. In order to obtain more PD for the solution of elevation and azimuth, it is necessary to switch the antenna to obtain PD. Therefore, the antenna switching operation is performed in the switch slot. Then IQ sampling is performed in the sample slot [12].

By the function of IQ sampling, the phase at the sampling instant may be determined by *atan* function (Eq.1) [12].

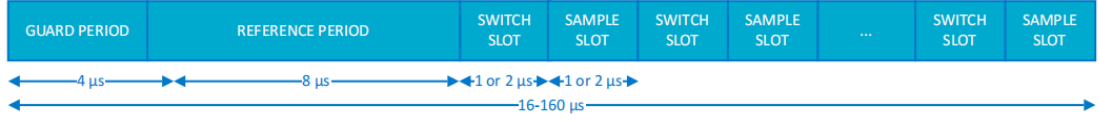


**Figure 3:** CTE structure [12]

$$\varphi' = \text{atan} \left( \frac{Q}{I} \right) \quad (1)$$

$\varphi'$  is the phase of the antenna.  $I$  is the value of the in-phase component.  $Q$  is the value of the quadrature component.

The angle can be calculated using the following Eq.2 [12].

$$\theta = \arccos \left( \frac{\psi \lambda}{2\pi d} \right) \quad (2)$$

In Eq.2,  $\theta$  is the angle of arrival. The  $\psi$  is the phase difference (PD) between antennas. The  $d$  is the distance between the antennas. The  $\lambda$  is the wavelength of the Bluetooth signal.

Before calculating the tag location point, it is also necessary to decompose the AoA into elevation and azimuth. Figure 4 shows an example of calculating the tag location point by elevation and azimuth. In the case of two AoA Locator, the three-dimensional coordinates of the tag can be known.

$$x = h \times \tan \left( \frac{e \times \pi}{180} \right) \times \cos \left( \frac{a \times \pi}{180} \right) \quad (3)$$

$$y = h \times \tan \left( \frac{e \times \pi}{180} \right) \times \sin \left( \frac{a \times \pi}{180} \right) \quad (4)$$

, where  $x$  and  $y$  are tag location points. The  $h$  is the height of the AoA locator relative to the tag plane. The  $e$  is the elevation. The  $a$  is the azimuth [12].

## 4. Mean Optimization Filter Design

The Kalman filter is one of the most important and common estimation algorithms. The Kalman filter produces estimates of hidden variables based on inaccurate and uncertain measurements [13]. ME is the unfiltered elevation. MA is the unfiltered azimuth. KE is the elevation after using Kalman filter. KA is the azimuth after using Kalman filter.

Figure 5 shows the data of ME, MA, KE, and KA in time series at the same location point are unstable. The collection time is 3 seconds. The x-axis represents the index of data that is the time of measurement. The y-axis represents the angle. Figure 5 shows the fluctuation amplitude of KE and KA is small. The fluctuation amplitude of MA is the largest. Figure 5 shows that KA has a good filtering effect and can filter the noise in ME. Not only that, for ME, the filtering

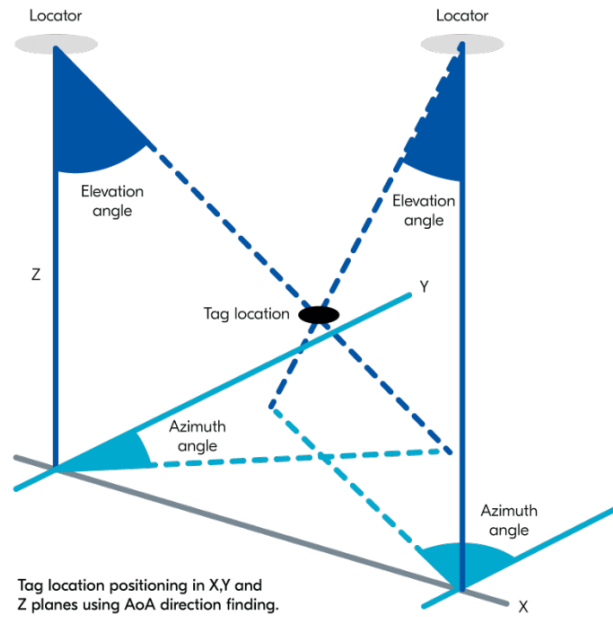


Figure 4: Calculating a tag location point using elevation and azimuth [12]

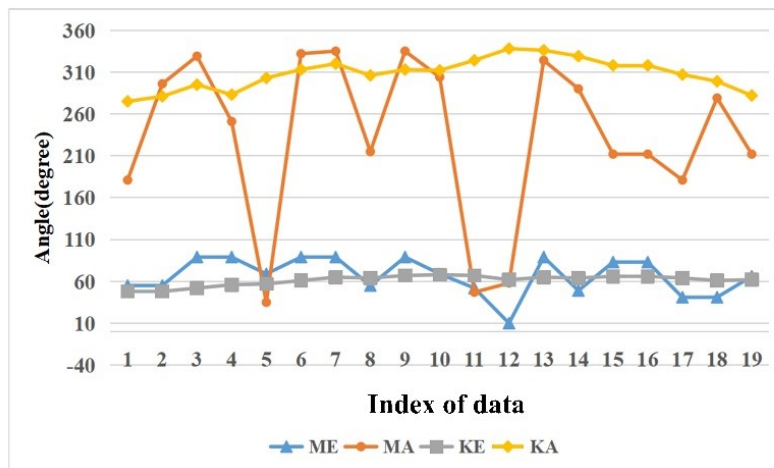
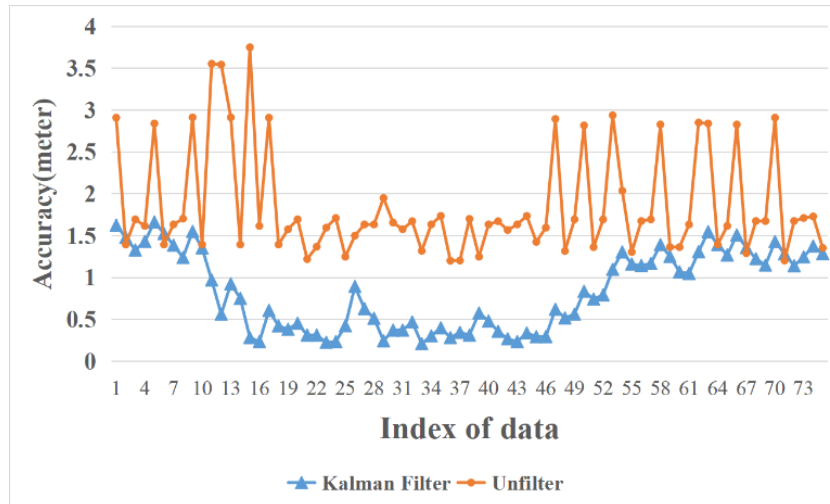


Figure 5: The data of ME, MA, KE, and KA in time series [14]

effect of KE is also good. Figure 5 shows that the Kalman filter can remove the noise effectively. However, in our actual tests, the localization results of the Kalman filter are very unstable.

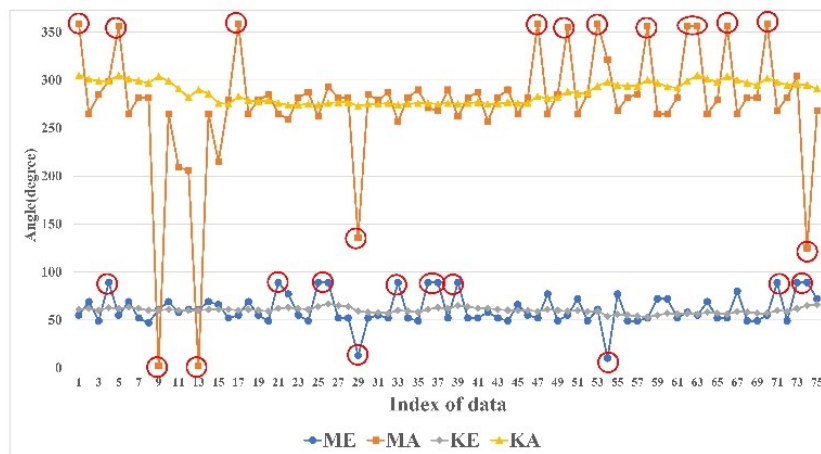
Figure 6 shows the errors of the localization results calculated by Eq.3 and Eq.4, using ME, MA, KE, and KA. The x-axis represents the index of data that is the time of measurement. The y-axis represents accuracy (meter). Figure 6 shows that the error exhibits a random phenomenon and cannot always be minimized. This is the problem caused by the Kalman filter.

Figure 7 shows the ME and MA collected at the same location point for 10 seconds. The data



**Figure 6:** Positioning error of a location point after using Kalman filter

points marked by red circles in Figure 7 are outliers. The x-axis represents the index of data that is the time of measurement. The y-axis represents the angle. Figure 7 shows that there are many anomalies in the data. The descriptive statistical analysis of ME and MA shows many anomalies in ME and MA with abrupt decreasing values. Also, many outliers with a value of 89 degree are found in ME, and many outliers with a value of 359 degree are found in MA. It is worth noting that the range of elevation is 0 degree to 90 degree, and the range of azimuth is 0 degree to 360 degree.



**Figure 7:** Examples of anomalies for ME and MA

ME and MA belong to time series data. In this paper, a test is performed using a method specifically designed to find outliers in time series data, which is named the generalized (Extreme Studentized Deviate) ESD test [15]. It detects one or more outliers in a univariate data set. Given

the upper bound,  $r$ , the generalized ESD test essentially performs  $r$  separate tests: a test for one outlier, a test for two outliers, and so on up to  $r$  outliers.

Figure 8 and Figure 9 show the results of anomaly identification for ME and MA data at a location point using the ESD method. The x-axis represents the index of data that is the time of measurement. The y-axis represents the angle. The points marked in red in Figure 8 and Figure 9 are the outliers identified by the ESD method. Figure 9 shows that all low-value outliers are correctly identified, but high value outliers such as 89 degree in ME and 359 degree in MA are not correctly identified. In addition, when these anomalies appear at fixed intervals, ESD considers them as normal points and cannot effectively perform anomaly recognition. This is the problem of ESD.

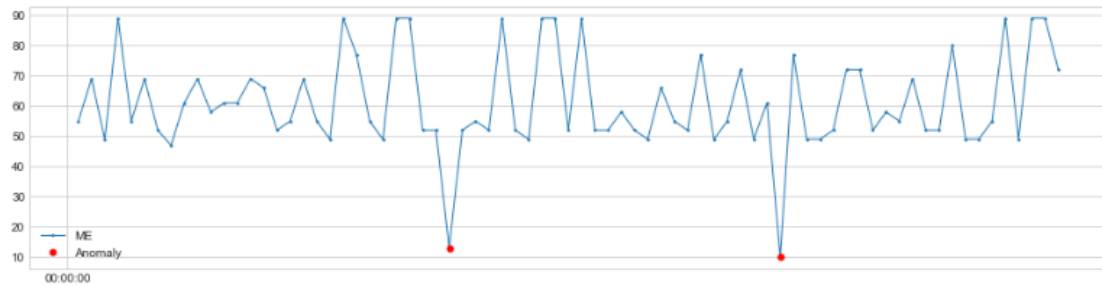


**Figure 8:** Identification of anomalies in ME by ESD

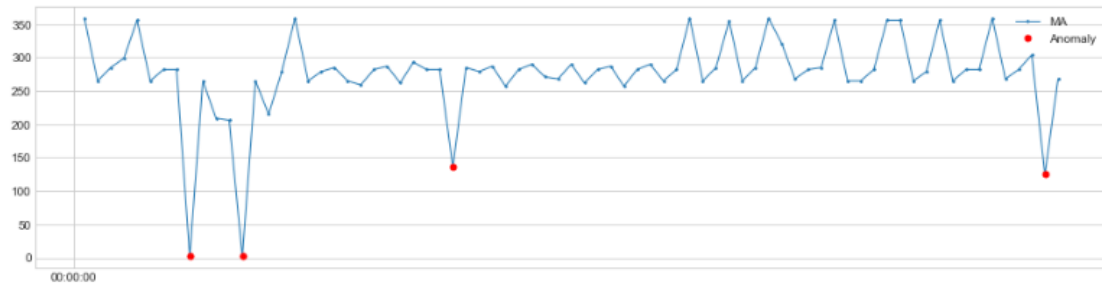


**Figure 9:** Identifying the anomalies of MA by ESD

The mean optimization filter algorithm process is shown in Figure 10. In the first step, the set of angles is obtained as  $A$ . In the second step, the anomalies in  $A$  are identified by the box plot method, and the anomalous data are removed. In the third step, the average of  $A$  is calculated as the optimal average. Step 4, generate all possible intervals of  $A$  as  $R$ . Step 5, calculate the set of interval length of each interval in  $R$  as  $N$ . Step 6, sort  $N$  in ascending order according to the magnitude of interval length. Step 7, check whether the interval contains the optimal average according to the order of  $N$ . If the current interval contains the optimal average, the interval is chosen. Otherwise, check the next interval. Step 8, calculate  $P_{right}$  and  $P_{left}$  according to the optimal average. Step 9, calculate  $C_{right}$  and  $C_{left}$  corresponding to  $P_{right}$  and  $P_{left}$  respectively. Step 10, if  $C_{right}$  is greater than  $C_{left}$ , the left interval of the chosen interval is the

current optimal average. If  $C_{right}$  is smaller than  $C_{left}$ , the right interval of the chosen interval is the current the optimal average. Step 11, the average of the new interval is updated to the optimal average. Step 12, if the optimal average does not change, the current optimal average is output. Otherwise, return to step 8.

1. Obtain the set of angles as  $A$
2. Use the box plot method to identify the outliers in  $A$ , and remove them
3. Determine the average of  $A$  as the optimal average
4. Calculate all possible intervals of  $A$  as  $R$
5. Determine the number of interval length between each interval in  $R$  as  $N$
6. Sort  $N$  in ascending order based on the number of interval length
7. According to the order of  $N$ , determine whether the interval contains the optimal average. If the current interval contains the optimal average, then it is the chosen interval. Otherwise, the next interval is considered
8. Using the optimal average,  $P_{right}$  and  $P_{left}$  are calculated
9. Calculate the  $C_{right}$  and  $C_{left}$  corresponding to  $P_{right}$  and  $P_{left}$ , respectively
10. If  $C_{right}$  is greater than  $C_{left}$ , then the left interval of the chosen interval is the current optimal average. If  $C_{right}$  is less than  $C_{left}$ , then the right interval of the chosen interval is the current optimal average
11. The optimal average is updated to the average of the new interval
12. If the optimal average does not change, the current optimal average is output. Otherwise, proceed to step 8.

**Figure 10:** The procedure of mean optimization filter algorithm

A box plot is a method of illustrating the locality, spread, and skewness of numerical data through their quartiles in descriptive statistics [15]. Also, the box plot method can be applied to outlier detection.

The dataset needs to be sorted in ascending order. One-quarter of the ordered data set is represented by the first quartile ( $Q1$ ). The third quartile ( $Q3$ ) represents three-quarters of the data set. This paper's  $Q1$  and  $Q3$  are 25th percentile and 63rd percentile, respectively. The 63rd percentile is set based on the observed distribution of outliers for ME and MA. An interquartile range, or  $IQR$ , can be determined by subtracting the first quartile value ( $Q1$ ) from the third quartile value ( $Q3$ ). The  $IQR$  is shown in Eq.5 [16].

$$IQR = Q3 - Q1 \quad (5)$$

In this paper, the upper bound and lower bound are calculated to identify the anomalies in the data set. The upper bound and lower bound are shown in Eq.6 and Eq.7, respectively.

$$UP = Q3 + C_1 \times IQR \quad (6)$$

$$LOW = Q1 - C_2 \times IQR \quad (7)$$

In this paper, the values of  $C_1$  and  $C_2$  are finally determined through a comparative analysis of experimental data. In this paper,  $C_1$  is 0, and  $C_2$  is 0.5. Any data point in the dataset that is larger than the upper bound or smaller than the lower bound is considered an outlier.

To find the optimal elevation and azimuth in the data set, a mean optimization filter is proposed in this paper. The box plot method is used to identify the anomalies. The anomalies greater than the upper and lower bound are removed from the data set. Due to noise, the ME and MA change with time in the case of the same location point. Then finding the optimal



elevation and azimuth in ME and MA becomes the goal of this paper. As shown in Eq.8,  $A$  is the unduplicated angle dataset after filtering out the outliers.

$$A = [A_1, A_2, A_3 \dots \dots, A_n] \quad (8)$$

, where  $A_n$  represents the  $n_{th}$  angle. Interval is the difference between two angles in  $A$ . Two different angles can form each interval in order to find the optimal average, all possible intervals in  $A$  need to be generated, as shown in Eq.9.

$$R = [(A_1, A_2), (A_1, A_3), (A_2, A_3) \dots \dots, (A_{n-1}, A_n)] \quad (9)$$

, where  $R$  is the set of all possible intervals of  $A$ . Each interval length needs to be calculated, as shown in Eq.10.

$$N = [|A_1 - A_2|, |A_1 - A_3|, |A_2 - A_3| \dots \dots, |A_{n-1} - A_n|] \quad (10)$$

, where  $N$  is the set of interval length for each interval.  $|A_r - A_s|$  denotes the interval length between  $A_r$  and  $A_s$ . In  $N$ , each interval length is sorted in ascending order. The core idea of this paper is to determine the optimal average by repetitively narrowing the range of the interval. The average of  $A$  is called the optimal average (*Average*). The optimal average is updated repetitively in the next step. The following steps aim to narrow the interval to find the optimal average. This paper considers the decision basis of distinguishing the data points to the left and right of the optimal average as one of them.

$$P_{right} = \{A_k \mid A_k > Average\} \quad (11)$$

$$P_{left} = \{A_l \mid A_l < Average\} \quad (12)$$

, where  $P_{right}$  is the set of angles greater than *Average*, and  $P_{left}$  is the set of angles less than *Average*. To find the optimal average more accurately, this paper uses the standard deviation between  $A_i$  and *Average* as one of the decision bases to find it.  $C$  is the criterion to divide  $A$  into two sets in order to find a subset in which more optimal average may exist.

$$C = \frac{1}{\sqrt{\frac{\sum(A_i - Average)^2}{N}}} \quad (13)$$

, where  $C$  is the inverse of the standard deviation.  $N$  is the size of  $[A, A_2, A_3 \dots \dots, A_i]$ .  $A_i$  is the  $i_{th}$  angle. The larger  $C$  means that  $A_n$  is closer to *Average*. Then the interval closer to *Average* is used to find the optimal average.

To further introduce our proposed MOF, this paper illustrates how the proposed method works through an example in Figure 11 and Figure 12. As shown in Figure 11, we assume that  $A$  is a set of  $A_1, A_2$ , and  $A_3$  and takes values from 0 to 360 degrees. *Average* is calculated from  $A$ .  $R$  is a set of  $(A_1, A_2)$ ,  $(A_1, A_3)$ , and  $(A_2, A_3)$ , denoted as the example by Interval 1, Interval 2, and Interval 3, respectively. Each interval length needs to be calculated. The interval length 1, interval length 2, and interval length 3 form  $N$ . In the next step,  $R$  is sorted by  $N$  in ascending order. Starting from the first interval in  $N$ , this paper determines whether the current interval

contains an *Average*, if so, the current interval is used to find the optimal average; if not, start to determine the next interval.

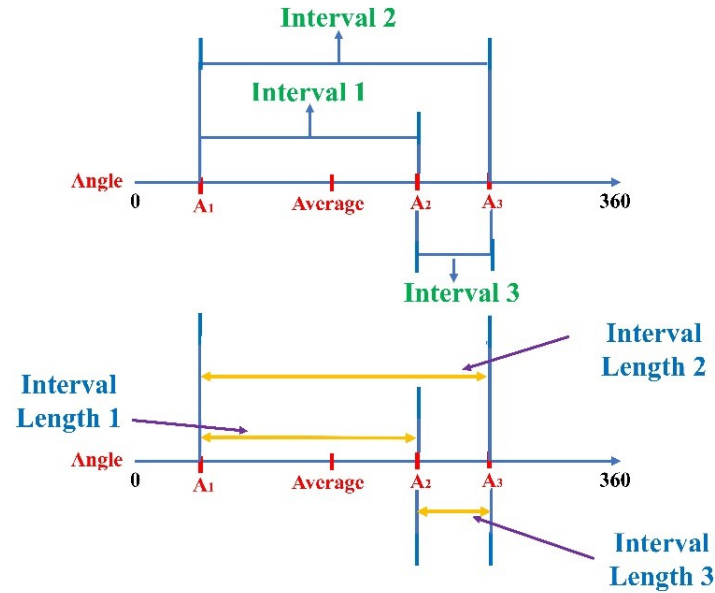


**Figure 11:** Process of determining the shortest interval

Figure 12 illustrates the process of determining the optimal average. This paper assumes that Interval 1( $A_1, A_2$ ) contains the optimal average. In the next step, the data points to the left and right of the *Average* need to be identified. In the Figure 12,  $P_{right}$  is  $A_2, A_3$ , and  $P_{left}$  is  $A_1$ . Calculate the  $C_{right}$  and  $C_{left}$  corresponding to  $P_{right}$  and  $P_{left}$  respectively by Eq.13. In Figure 12,  $C_{right}$  is larger than  $C_{left}$ . Therefore, the left interval of ( $A_1, A_2$ ) becomes the current *Average*( $M$ ), and the right interval is  $A_2$ . The optimal average is updated to the average of  $M$  and  $A_2$ . This cycle is repeated until the optimal average does not change.

## 5. Performance Evaluation

HANNARA is a Korea Maritime and Ocean University student training ship. Figure 13 depicts the layout of the HANNARA ship's student living quarters. The purpose of showing a plan of the HANNARA is that the ship environment is similar to that of a cruise ship, and there are enough persons on board as well. From Figure 13, the ship space is narrow and the multipath effect can be more intense in the ship indoor environment. Compared with the indoor environment on land, the spatial distribution structure of the ship's interior can make the received data contain more noise. The indoor positioning techniques studied for the ship environment can also be used for other indoor environments [17].

In order to avoid the risk of COVID-19 infection to students on HANNARA, a classroom with a similar structure to one of the cabins on HANNARA is found as an experimental environment

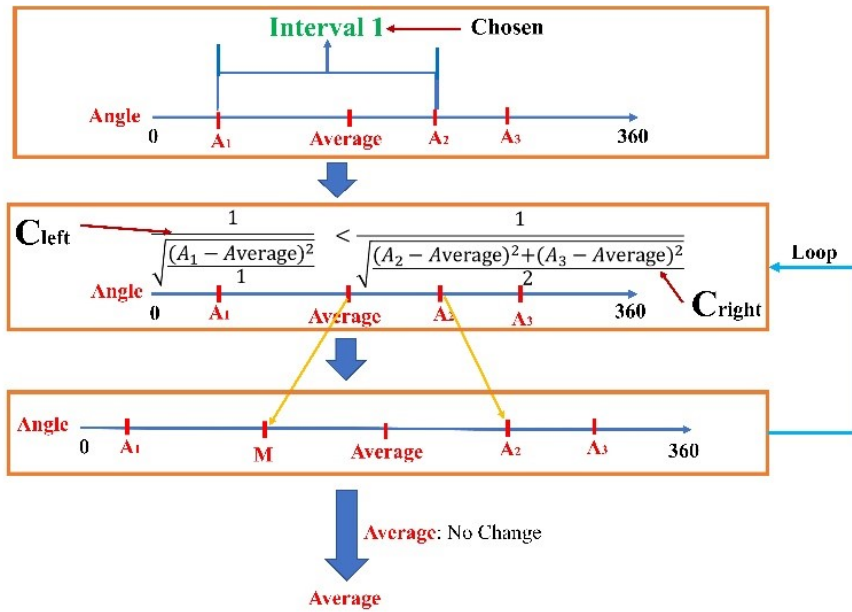


Figure 12: Process for determining the optimal average

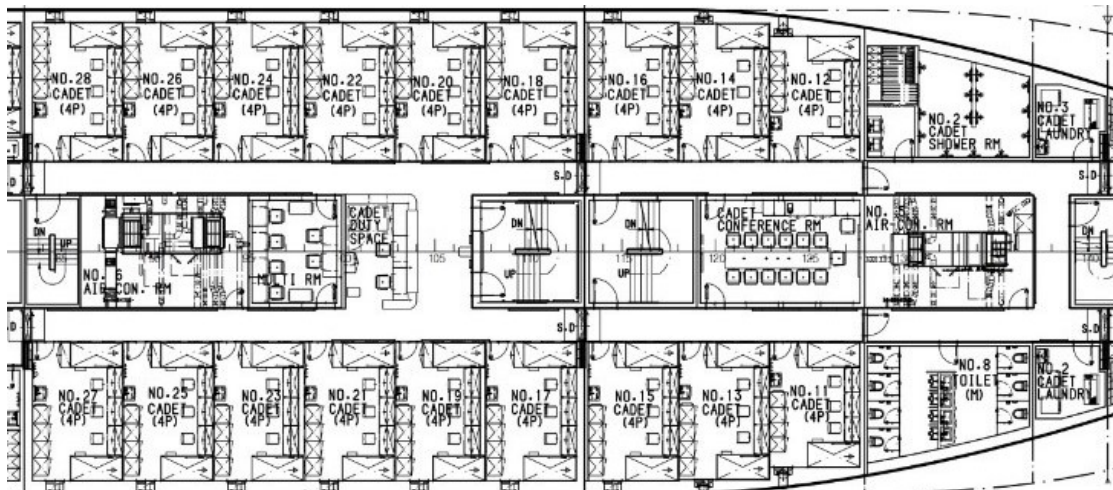


Figure 13: The floor plan of main deck in the HANNARA ship [17]

in the room. Meanwhile, the classroom tables and chairs can reflect signals. Therefore, the indoor environment of the classroom is similar to that of a ship. We plan to conduct testing in the ship environment after the risk of COVID-19 infection is minimized. Figure 14 shows the experimental environment of this paper. A classroom of 7.6 m in length and 7.85 m in width is chosen for testing. This paper uses a USB cable to transfer data from the AoA Locator to a python program on the computer to do location points calculations. Because  $h$  is the height of

the AoA locator relative to the tag plane. In this paper,  $h$  is set to 1.5 m.



**Figure 14:** Experiment environment [14]

Figure 15 shows the AoA Locator used in this paper. The AoA Locator has 12 antennas. The Bluetooth signal from the tag can be received from all directions by AoA Locator. It is able to calculate the location point of the tag by using one AoA Locator. The AoA Locator uses Nordic Semiconductor's nRF52833 chip [16]. The following is the experimental environment for this paper: CPU is AMD Ryzen 7 5700G (3.8GHz), RAM is 32 GB, OS is Windows 11 21H2, Visual Studio Code version is 1.61.2, Python version is 3.8. The number of ME and MA is 75 collected on user locations in 10 seconds.

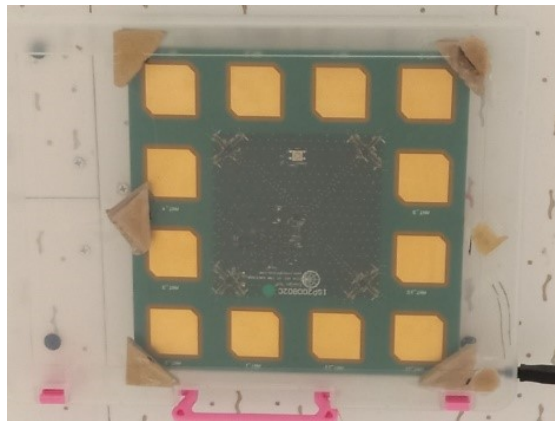


**Figure 15:** AoA Locator [14]

To test the AoA indoor positioning accuracy, 9 user location points are randomly chosen. Figure 16 shows the distribution of the AoA Locator and 9 user location points (Tag). The red dots represent the location point of the AoA Locator [14].

This paper compares five different filters. They are Box Plot-Remove, Box Plot-Modify, KF,

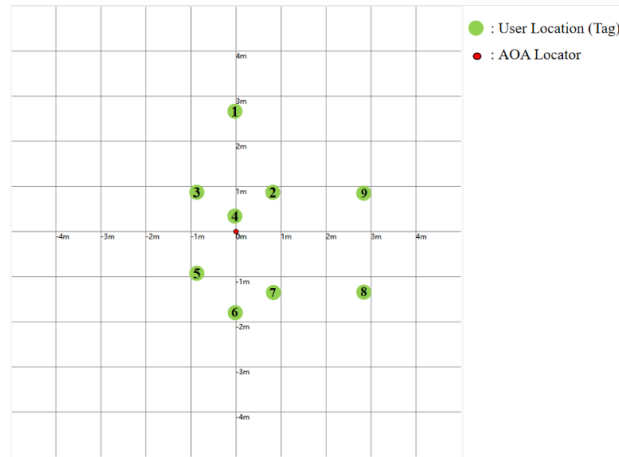


**Figure 16:** Distribution of user location points (Tag)

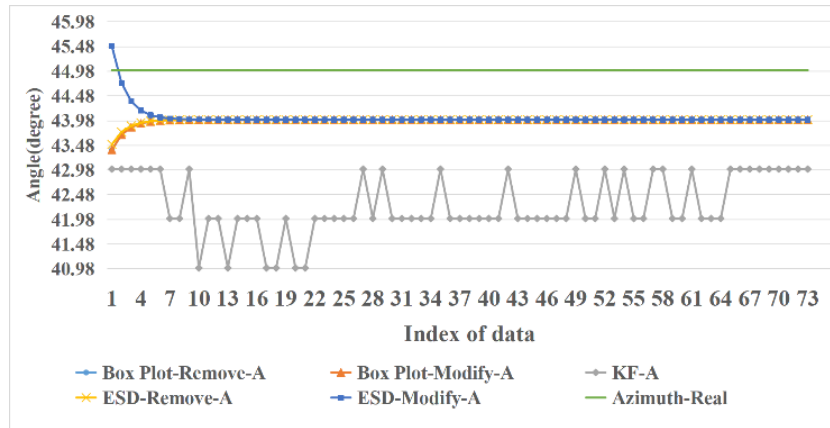
ESD-Remove, and ESD-Modify. Box Plot-Remove that removes the outlier after identifying it with the box plot method. KF is Kalman filter. ESD-Remove that removes anomalies after identifying them by ESD method. ESD-Modify those correct anomalies with low values after identifying them by ESD method. The correction method is 90 minus angle for elevation and 360 minus angle for azimuth. “-E” is elevation. “-A” is azimuth.

Figure 17 shows the filtering effect of different filters combined with MOF on the elevation of user location point 9. The x-axis represents the index of data that is the time of measurement. The y-axis represents the angle. Elevation-Real is the real elevation. The filtering effect of KF-E presents a random characteristic, which is not stable close to the real elevation. Box Plot-Modify-E, KF-E, ESD-Remove-E, and ESD-Modify-E all show a tendency to move away from the true elevation and eventually reach a fixed value. Box Plot-Remove-E has the best filtering effect, gradually moving closer to the true elevation and eventually reaching a fixed value.



**Figure 17:** Calculation results of different filters for elevation (user location point 9)

Figure 18 shows the filtering effect of different filters combined with MOF for azimuth at user location point 9. The x-axis represents the index of data that is the time of measurement. The y-axis represents the angle. Azimuth-Real is the real azimuth. Meanwhile, the filtering effect of KF-A shows a random characteristic. And the filtered result is farthest from the real azimuth. Box Plot-Modify-A and ESD-Remove-A first gradually approach the real azimuth and then stabilize. Box Plot-Remove-A and ESD-Modify-A have the same filtering effect, first passing through the real azimuth and finally reaching a fixed value. In this case, Box Plot-Remove-A and ESD-Modify-A have the best result.



**Figure 18:** Computational effect of different filters on azimuth (user location point 9)

Figure 19 shows the indoor positioning accuracy using MOF with different filters. The x-axis represents the user location point and the y-axis represents the accuracy. Figure 19 shows that the Box Plot-Remove combined with MOF for user location point 1, 2, 4, 6, 8 and 9 has greatly improved the indoor positioning accuracy. The improvement in indoor positioning accuracy at user location point 3 and user location point 7 is not obvious. There is no contribution to the localization accuracy improvement at user location point 5. We think that  $Q1$  and  $Q3$  need to be further optimized to exclude outliers as much as possible to further improve the outlier identification. Overall, the Box Plot-Remove combined with MOF method has greatly improved the localization accuracy.

Based on the results shown in Figure 17 and Figure 18, this paper finally adopts the Box Plot-Remove method for the anomalies. As shown in Figure 16, ME and MA from AoA Locator are collected at 9 user location points. The anomalies of ME and MA are identified by the Box Plot-Remove method. The optimal average of ME and MA is calculated using MOF. Its calculation results are combined with Eq.3 and Eq.4 to calculate  $x$  and  $y$ . The RMSE (Root-mean-square error) is calculated by comparing the true  $x$  and  $y$ . The RMSE of Box Plot-Remove is 0.34 m. The RMSE of Box Plot-Modify is 0.55 m. The RMSE of KF is 0.61 m. The RMSE of ESD-Remove is 0.42 m. The RMSE of ESD-Modify is 0.56 m. Among them, Box Plot-Remove combined with MOF gives the best results.

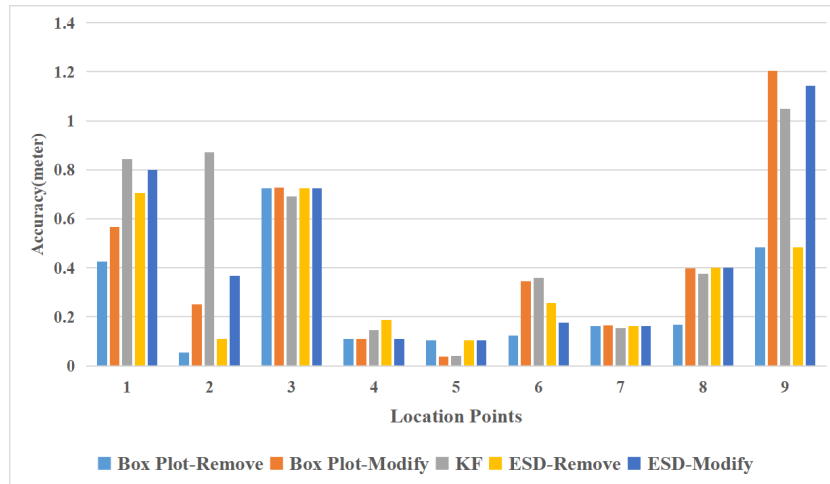


**Figure 19:** Indoor positioning accuracy using MOF with different filters

## 6. Conclusion

The narrow space in the ship environment increases the multipath effect. Elevation and azimuth are the two most important parameters in Bluetooth 5.1 AoA indoor positioning algorithm, and the inaccuracy of elevation and azimuth can increase the indoor positioning error dramatically. In order to find the most accurate elevation and azimuth, this paper proposes a MOF to determine the optimal elevation and azimuth in ship environments. The shortest interval of true elevation and azimuth is determined by calculating the average. Finally, the optimal elevation and azimuth are determined by continuously narrowing the range of the shortest interval. The experiment is conducted in a classroom with a similar structure to a HANNARA ship cabin. The AoA Locator of Nordic Semiconductor's nRF52833 chip is used. Five different filters is combined with MOF are tested on 9 user location points. The final results show that Box Plot-Remove is combined with MOF has the highest accuracy with an RMSE of 0.34 m. The indoor positioning accuracy is effectively improved. We plan to conduct testing in the ship environment after the risk of COVID-19 infection is minimized.

## Acknowledgments

This research was supported by Basic Science Research Program through the National Research Foundation of Korea (NRF) funded by the Ministry of Education (grant number: 2021R1I1A3056125).

## References

- [1] N. Klein, International law perspectives on cruise ships and covid-19, *Journal of international humanitarian legal studies* 11 (2020) 282–294.

- [2] B. Batista, D. Dickenson, K. Gurski, M. Kebe, N. Rankin, Minimizing disease spread on a quarantined cruise ship: A model of covid-19 with asymptomatic infections, *Mathematical biosciences* 329 (2020) 108442.
- [3] E. Fanoy, A. E. Ummels, V. Schokkenbroek, B. van Dijk, S. Wiegmans, T. Veenstra, A. A. van der Eijk, R. S. Sikkema, A. de Raad, Outbreak of covid-19 on an industrial ship, *International Maritime Health* 72 (2021) 87–92.
- [4] G. Pau, F. Arena, Y. E. Gebremariam, I. You, Bluetooth 5.1: An analysis of direction finding capability for high-precision location services, *Sensors* 21 (2021) 3589.
- [5] C. Huang, Y. Zhuang, H. Liu, J. Li, W. Wang, A performance evaluation framework for direction finding using ble aoa/aod receivers, *IEEE Internet of Things Journal* 8 (2020) 3331–3345.
- [6] A. Koutris, T. Siozos, Y. Kopsinis, A. Pikrakis, T. Merk, M. Mahlig, S. Papaharalabos, P. Karlsson, Deep learning-based indoor localization using multi-view ble signal, *Sensors* 22 (2022) 2759.
- [7] F. A. Toasa, L. Tello-Oquendo, C. R. Peñafiel-Ojeda, G. Cuzco, Experimental demonstration for indoor localization based on aoa of bluetooth 5.1 using software defined radio, in: *2021 IEEE 18th Annual Consumer Communications & Networking Conference (CCNC)*, IEEE, 2021, pp. 1–4.
- [8] X. Qiu, B. Wang, J. Wang, Y. Shen, Aoa-based ble localization with carrier frequency offset mitigation, in: *2020 IEEE International Conference on Communications Workshops (ICC Workshops)*, IEEE, 2020, pp. 1–5.
- [9] N. Paulino, L. M. Pessoa, A. Branquinho, E. Gonçalves, Evaluating a novel bluetooth 5.1 aoa approach for low-cost indoor vehicle tracking via simulation, in: *2021 Joint European Conference on Networks and Communications & 6G Summit (EuCNC/6G Summit)*, IEEE, 2021, pp. 259–264.
- [10] Z. Hajiakhondi-Meybodi, M. Salimibeni, A. Mohammadi, K. N. Plataniotis, Bluetooth low energy-based angle of arrival estimation in presence of rayleigh fading, in: *2020 IEEE International Conference on Systems, Man, and Cybernetics (SMC)*, IEEE, 2020, pp. 3395–3400.
- [11] S. Monfared, A. Delepaut, M. Van Eeckhaute, P. De Doncker, F. Horlin, Iterative localization method using aoa for iot sensor networks, in: *2019 IEEE 89th Vehicular Technology Conference (VTC2019-Spring)*, IEEE, 2019, pp. 1–6.
- [12] N. Semiconductor, nwp036 - direction finding, 2022. URL: [https://infocenter.nordicsemi.com/index.jsp?topic=%2Fnwp\\_036%2FWP%2Fnwp\\_036%2Fintro.html](https://infocenter.nordicsemi.com/index.jsp?topic=%2Fnwp_036%2FWP%2Fnwp_036%2Fintro.html).
- [13] H. Wood, N. Johnson, M. Sachdev, Kalman filtering applied to power system measurements relaying, *IEEE Transactions on Power Apparatus and Systems* (1985) 3565–3573.
- [14] H. Shin, Q. Lin, J. Son, An analysis of the accuracy of bluetooth 5.1-based aoa indoor positioning algorithms for ship passengers' health, in: *2022 Korea Multimedia Society Conference*, Korea Multimedia Society, 2022, pp. 1–4.
- [15] B. Rosner, Percentage points for a generalized esd many-outlier procedure, *Technometrics* 25 (1983) 165–172.
- [16] F. Hartwig, B. E. Dearing, *Exploratory data analysis*, 16, Sage, 1979.
- [17] Q. Lin, J. Son, Analysis of bluetooth rssi for proximity detection of ship passengers, *Applied Sciences* 12 (2022) 517.